This article has been accepted for publication in IEEE Transactions on Nuclear Science. This is the author's version which has not been fully edited and content may change prior to final publication. Citation information: DOI 10.1109/TNS.2024.3353489

Simulating Optical Single Event Transients on Silicon Photonic Waveguides for Satellite Communication

Giulio Terrasanta, Marcin W. Ziarko, Nicola Bergamasco, Menno Poot and Juraj Poliak

***Abstract*—Photonic integrated circuits are a promising platform for space applications. In particular, they have the potential to reduce the cost, size, weight and power consumption of satellite payloads that employ free-space optical communication. However, the effect of the space environment on such circuits has yet to be fully understood. Here, a simulation framework to investigate the impact of heavy ions on a silicon photonic waveguide is presented. These high-energy particles temporarily increase the waveguide losses, resulting in a drop of the transmitted power, commonly defined as either optical single event transient or single event effect. The magnitude and rate of such transients are simulated. The framework is based on three open source tools: OMERE, Geant4 and Meep. First, the heavy ion fluxes are modelled for commonly used satellite orbits. Afterwards, Monte Carlo simulations are used to generate realistic ion tracks and their effect is evaluated with 3D finite-difference time-domain simulations. The results show that single event effects have only a small impact on the transmission properties of silicon waveguides in the simulated orbits, thus indicating the potential of using silicon photonic integrated circuits in the space environment. Furthermore, the importance of having realistic carrier distributions, compared to using only an analytical model, is discussed.**

***Index Terms*—silicon photonics, single event effects, heavy ion, ion track, radiation effects, free space optical communication, satellite communication**

I. Introduction

THE interest in free space optical communication (FSOC) has rapidly grown in the recent years, particularly its application to satellite communication [1]–[5]. Thanks to the high data rates provided by optical links, satellite networks based on FSOC have the potential to complement the existing fiber network and to provide global broadband access [6], [7]. The deployment of this technology can be facilitated by using photonic integrated circuits (PICs), as they not only allow the integration of the required optical components on a single chip, but also they reduce the overall cost, size, weight and power (C-SWaP) [8], [9]. Furthermore, the use of PICs provide access to other physical processes, such as microresonator-based combs for massively parallel optical communication [10], [11]. PICs have already been successfully and widely used in fiber optic communication [12], [13]. However, space-based PICs are a more recent topic of research [14]. One of the challenges for space-based systems is the inherent radiation environment [15], the influence of which on integrated photonics is not yet fully understood.

One of the main radiation effect types are single event effects (SEEs), which are usually caused by heavy ions. These ions travel through the material and release their energy by generating a high density of electron-hole pairs (EHPs). In electronics, this leads to a charge diffusion and collection problem that has been extensively studied [16]–[18]. In photonics, the excess carrier concentration temporarily increases the material optical loss due to free carrier absorption (FCA) [19]. This results in a transient optical power disruption, that lasts until the EHP density returns to its original value. In a PIC for FSOC, this means a lower transmitted or received power of the optical link, potentially resulting in data loss. Due to the inherently dynamic nature of this effect and the need to analyze the overlap between the generated carriers and the optical mode, the theoretical and experimental research has been challenging. As detailed in [14], fewer studies have been performed compared to the two other main radiation effects: total ionizing dose (TID) and displacement damage (DD). Nevertheless, some advancements have been achieved in the recent years. A theoretical method to simulate the loss on a Si photonic waveguide at the time of the impact was first proposed in [20], while the loss transient after the impact was modeled in [21], [22]. Furthermore, a simulation methodology has been proposed to scale the simulation effects from the device level, such as a waveguide, to the system level [23]. First experimental measurements using laser-induced carriers were performed in [21], [24]. In [24], the phenomenon was defined as optical single event transient (OSET), to highlight that the impact of this physical process is limited to the optical domain, while SEEs are commonly associated with the radiation effects on electronics. Both a laser-induced experiment [25] and an ion-induced experiment [26] were conducted on waveguide-integrated SiGe photodiodes. Although simulation results prove that in principle a 100% loss is possible [24], some of these studies showed that losses higher than 10% are unlikely [20], [21]. Therefore, the real impact of OSETs is still unclear.

Previous studies were based on simulated tracks of a few selected ions, e.g. C and Kr [20], on analytical Gaussian dis-

G. Terrasanta is with the German Aerospace Center, Oberpfaffenhofen, 82234 Weßling, Germany and with the Department of Physics, TUM School of Natural Sciences, Technical University of Munich, Garching, Germany (e-mail: giulio.terrasanta@dlr.de).

M. W. Ziarko, N. Bergamasco and J. Poliak are with the German Aerospace Center, Oberpfaffenhofen, 82234 Weßling, Germany.

M. Poot is with the Department of Physics, TUM School of Natural Sciences, Technical University of Munich, Garching, Germany, with the Munich Center for Quantum Science and Technology (MCQST), Munich, Germany and with the Institute for Advanced Study, Technical University Munich, Garching, Germany.

This article has been accepted for publication in IEEE Transactions on Nuclear Science. This is the author's version which has not been fully edited and content may change prior to final publication. Citation information: DOI 10.1109/TNS.2024.3353489

tributions of the carriers [22], or on laser-induced EHPs [21], [24], [25], but not on a specific radiation environment with its heavy ions. Instead, for satellite communication applications, having accurate predictions of the expected loss for a specific satellite mission, i.e. a specific orbit and duration, is critical for the optical link power budget [4]. Furthermore, it would allow to reduce the C-SWaP of the communication payload, e.g. by selecting the appropriate metal shielding thickness, thus saving weight and space. To achieve this, a more comprehensive analysis is needed, that not only includes all the necessary heavy ions, but also uses realistic carrier distributions.

In this paper, we present a framework for simulating the expected losses and OSET rates in photonic devices for a given satellite orbit. For the photonic device, we simulate a silicon photonic waveguide, which is the basic building block of any Si PIC. For the orbits, we consider orbits commonly used in navigation and communication systems. In this framework, each satellite orbit is first analyzed to find the typical ions of its radiation environment. Afterwards, the EHP initial distributions generated by those ions are simulated. The simulated carrier tracks are then used in finite-difference-time-domain (FDTD) simulations to find the resulting optical loss. Finally, the OSET magnitudes and rates are calculated for four typical satellite orbits. In addition, the relationship between optical loss and important radiation metrics, such as linear energy transfer (LET) and ion energy, is discussed.

The structure of the paper is the following. Section II describes the tools used in the simulation framework and shows some intermediate results to provide insight into each step of the framework. In Section III, the simulation results for all the ions present in the radiation environment are displayed and discussed, and the OSET rates are calculated. Finally, in Section IV, the results are summarized, and we draw conclusions from this work and discuss possible next steps.

II. Simulation Framework

A schematic representation of a heavy ion strike on a Si photonic waveguide is shown in Fig. 1. A buried waveguide surrounded by SiO_2 is considered. The waveguide width and height are $450\,\mathrm{nm}$ and $220\,\mathrm{nm}$, respectively, which are typical dimensions for such a waveguide [13]. In our simulations, only the case of a perpendicularly incident ion at the center of the waveguide is considered. If the heavy ion energy is high enough, the particle can pass through the satellite shielding and the cladding, and it can reach the Si waveguide. The energy released along its path generates an excess of EHPs, whose distribution depends on the heavy ion atomic number and its energy [27]. The generated EHP density locally affects the properties of the material, changing its refractive index and increasing the loss due to FCA, which can be modeled using the Drude theory [20]. The optical signal propagating through the waveguide is affected by these changes, resulting in a loss of signal due to absorption. Nevertheless, the carriers will then diffuse and the properties of the material will return to their nominal values.

To simulate all of these different phenomena, our framework leverages three open-source tools: OMERE [28], Geant4 [29] and Meep [30]. The dependencies between the different software are shown in Fig. 2. OMERE is used to simulate the radiation environment of the satellite orbit, and to obtain the heavy ion fluxes for different species and energies. The carrier distributions generated by these ions are then simulated using Geant4, where a typical Si photonic layer stack is considered for the simulation. The resulting distributions are converted into material properties, and used in Meep to perform FDTD simulations to calculate the optical loss in the device under study, which in this case is a buried channel waveguide. Finally, the information on the loss is combined with the ion fluxes to calculate the OSET amplitudes and rates. The use of the three tools is described in the subsections II-A, II-B, and II-C.

Before going into the details of the simulation framework, we would like to emphasize the two main simplifying assumptions that were taken.

1) This works considers only the initial carrier distribution, i.e. the distribution that is generated when the ion travels through the waveguide. As discussed in detail in [21], the initial carrier distribution is quickly smoothed out by ambipolar diffusion, in a time scale of about tens of picoseconds. Afterwards, the carrier dynamic is dominated by surface recombination, which operates in a time scale of tens of nanoseconds. Therefore, the simulated OSET magnitudes in this work, meaning the simulated losses, are only valid at the very beginning of the transient. However, even if the simulation framework only covers a short time scale, it is still able to evaluate

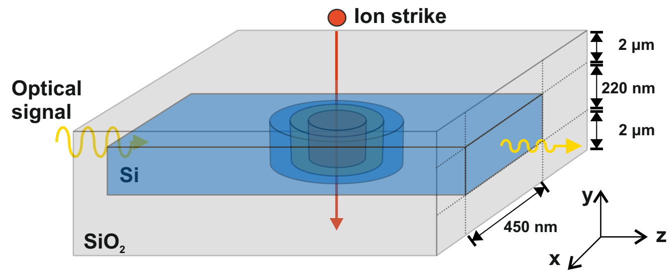

Fig. 1. Schematic representation of a Si photonic buried waveguide struck by a heavy ion while an optical signal is propagating. Waveguide width and height are noted, together with the cladding and substrate width. The drawing is not to scale.

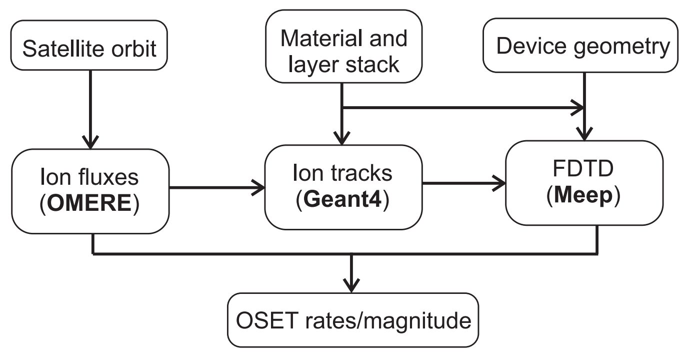

Fig. 2. Simulation framework flowchart. Information flow is represented with arrows.

the rate and initial magnitude of OSETs in a realistic scenario of a satellite payload in a specific orbit, which is a valuable indication for the development of silicon-based satellite communication payloads. For brevity, the *initial carrier distribution* is referred to only as *carrier distribution* in the remaining of the paper.

2) This work assumes that the whole ion flux is incident at the center of the waveguide and it is perpendicular to the waveguide's surface. In practice, ions would strike with any angle and on any point of the waveguide. While an angled trajectory is expected to induce a higher loss [21], the central position provides the largest overlap with the optical mode, and thus the highest losses, for a perpendicular trajectory [22]. Therefore, this simplification is useful to have a first approximation of the OSET magnitudes. Furthermore, this simplification greatly reduces the simulation effort, because each angled trajectory would need to be simulated both in Geant4 and in Meep, largely increasing the amount of simulations required.

A. Ion Fluxes Analysis

OMERE is an open source software for space environment and radiation effects, that computes the radiation environment for a given a satellite orbit [28]. In this paper, OMERE is used to create a dataset of ion fluxes $\Phi(Z,E)$ for a wide range of atomic numbers Z and energies E. Four different orbits are considered: a geostationary orbit, a medium Earth orbit used for the global navigation satellite system (GNSS, e.g. Galileo), and two low Earth orbits (LEOs), one corresponding to the international space station orbit, and one with a high altitude polar orbit that is planned for use in various commercial LEO satellite megaconstellations [31]. We define these orbits as *GEO*, *Galileo*, *LEO - ISS*, and *LEO - Pol*, respectively. These orbits are representative of typical satellite orbits and cover a wide range of altitudes. The orbit parameters are listed in Table I. After selecting the orbits, the particles radiation sources and their models need to be selected. For OSETs, protons ($Z = 1$) and ions ($Z > 1$) need to be included. Protons can be trapped in the magnetosphere or emitted by sun, while ions originate either from the sun or from galactic cosmic rays. The models for each particle are chosen using the ECSS standards [32], [33], that contain the rules to determine the radiation environment. The models are listed in Table II. The magnetosphere *Jensen-Cain* model is used. The satellite shielding is $1\,\mathrm{mm}$ of aluminium for all orbits. Even though higher altitude satellites are expected to have a thicker shielding than the lower altitude ones, choosing the same thickness allows us to compare the OSET rates later on. Element species from 1 ($^1_1$H) to 80 ($^{200}_{80}$Hg) are considered, even though the species abundance is expected to decreases with atomic number, with a steep drop for atomic numbers higher than $Z > 26$ [15].

As an example, Fig. 3(a) and Fig. 3(b) show some of the simulated differential fluxes $\frac{d\phi(Z,E)}{dE}$ for the orbits defined as *GEO* and *LEO-Pol*, respectively, including the solar flare contribution. Six out of the eighty ions are shown. As can be seen in both plots, H and He have the highest fluxes, thus being the most abundant ions in the Earth's radiation environment, and heavier ions have a significantly lower flux.

TABLE I
SATELLITE ORBIT PARAMETERS

Orbit	Inclination (°)	Altitude (km)
GEO	0	35784
Galileo	56	23222
LEO - Pol	98	800
LEO - ISS	51.5	400

TABLE II
SPACE RADIATION ENVIRONMENT MODELS

Particle	Model
Trapped protons	AP8 - Min.
Solar protons	ESP (80%)
Solar ions	Sapphire
Galactic cosmic rays	GCR ISO 15390 (solar minimum)
Flare protons	Worst 5 minutes October '89
Flare ions	CREME95 worst 5 minutes

In order to optimize the computational efforts, we want to reduce the number of elements to be simulated in the next steps. Therefore, the relative abundance $\mathrm{RA}(Z)$ of each ion is calculated using

$$\mathrm{RA}(Z) = \int_{E_a}^{E_b} \frac{d\phi(Z,E)}{dE} \times A\,dE, \tag{1}$$

where A is the PIC area and the energy range $E_a - E_b = 0.1$-$100\,\mathrm{MeV/amu}$ is chosen. As discussed later in Section III, this is the range where most of the interaction takes place for the considered layer stack. The results for the chosen PIC area ($A = 0.16\,\mathrm{cm}^2$, which is the typical area of transceiver chip used in the project reported in [9]) are shown in Fig. 3(c) and Fig. 3(d). In Fig. 3(c), the solar flare contribution is excluded, while it is included in Fig. 3(d). The relative abundances of orbits defined as *GEO* and *Galileo* are almost identical, while the orbits *LEO-Pol* and *LEO-ISS* have a lower abundance. When the solar flare contribution is taken into account, the RA of each ion is at least one order of magnitude larger. For more detailed studies, we define an arbitrary threshold of one event per year for the case without solar flare (Fig. 3(c)). Atomic numbers $Z > 35$ have a relative abundance below the defined threshold, so $Z = 35$ is defined as the heaviest element to be simulated in the next steps. In Fig. 3(d), this corresponds to a RA that is less than one per day, which is longer than the intended time scale of the used solar flare models, which are representative of the worst five minutes. Therefore the condition $Z > 35$ is meaningful for both cases.

B. Ion Tracks Simulations

Ion tracks are simulated using Geant4 [29], a Monte Carlo simulation toolkit for studying particle-matter interactions. Although analytical models of ion tracks have been developed [34], those simulated with Geant4 have been shown to be more accurate in the track core (first 10-20 nm) and in the LET estimation [27]. The application developed in this work is

This article has been accepted for publication in IEEE Transactions on Nuclear Science. This is the author's version which has not been fully edited and
content may change prior to final publication. Citation information: DOI 10.1109/TNS.2024.3353489

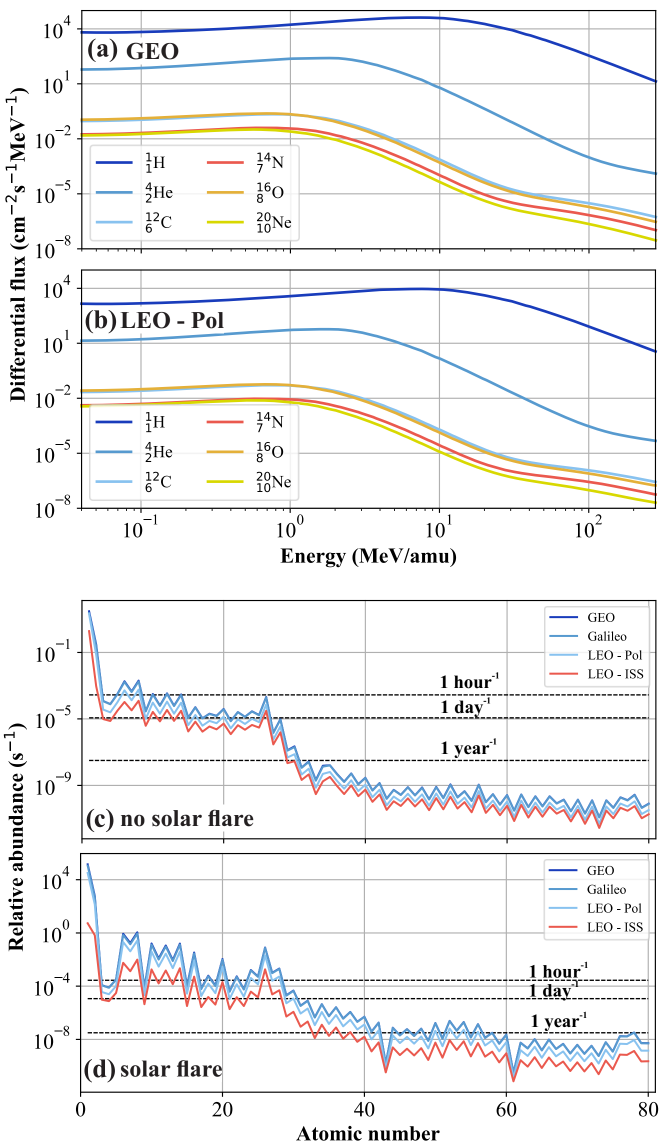

Fig. 3. (a-b) Examples of differential energy fluxes for six different ions in two different orbits, (a) *GEO* and (b) *LEO-Pol*, in the case of a solar flare. (c-d) Relative abundances of the element species. The solar flare contribution is considered only in in (d). The dashed horizontal line indicates thresholds of one event per year, one event per hour, and one event per day. The relative abundances of *GEO* and *Galileo* are overlapping.

based on a predefined advanced example called *microelectronics* [35]. The considered example uses the *MicroElec* models and processes, previously named *MuElec*, that are developed specifically for carrier generation by incident electrons, protons and ions [36]. Geant4 version 11 is used, which provides the latest version of the *MicroElec* package, which includes not only Si, but also other materials such as SiO_2 [37].

The goal of the simulation is to obtain the EHP density generated by each considered ion as a function of the radial distance from the ion path in the material. The material stack in the vertical direction (y-axis) is the one shown in Fig. 1, with the ion entering the simulation volume from the top. Since the lower SiO_2 layer is only needed for the ion to exit the Si layer and it has no impact on the simulation results, its thickness in this simulation is shortened from $2\,\mu\mathrm{m}$ to $280\,\mathrm{nm}$. In the x-z plane, we simulate a $2\,\mu\mathrm{m}\times 2\,\mu\mathrm{m}$ Si layer convering the entire plane: the waveguide width is still not taken into account, and it will be considered only at a later stage. Therefore, the simulation volume is $2\,\mu\mathrm{m}\times 2.5\,\mu\mathrm{m}\times 2\,\mu\mathrm{m}$ in the x-y-z directions, respectively. A monoenergetic beam is normally incident on the layer stack. As discussed in [27], a layer around $200\,\mathrm{nm}$ is thin enough for the track structure to be considered uniform, and thick enough to get good statistics. Therefore, we assumed that the track structure is constant along the vertical direction in the $220\,\mathrm{nm}$ thick Si layer, and only the transferred energy as a function of the distance from the ion path is stored. The carrier density is calculated by dividing the deposited energy by the EHP creation energy in Si, which is W_{eh}= $3.6\,\mathrm{eV}$ [27]. An average charge density $N(r)$ as a function of radial distance is calculated by simulating 1000 ions. This is repeated for the different energies and the different ions. Examples of $N(r)$ for ${}^{1}_{1}$H and ${}^{20}_{10}$Ne are shown in Fig. 4(a) and Fig. 4(b), respectively. Fig. 4(a-b) show that the charge density peaks near the ion path, and then decreases the further away from it. However, the exact geometry of the carrier distribution is highly dependent on the ion energy, or, more precisely, on its energy per atomic mass unit (amu), as explained in [27]. Heavy ions with the same energy per amu generate a similar shape, while the carrier concentration scales approximately with the square of the atomic number Z^2 [27]. This can be seen when comparing Fig. 4(a) and Fig. 4(b). In this case, $(Z_{Ne}/Z_H)^2 = (10/1)^2 = 100$, which can be seen in the plotted simulations.

An important metric that is commonly used in radiation studies is the LET, which is the amount of energy that an ionizing particle transfers to the material traversed per unit distance, divided by the material density. Assuming a vertical ion impact propagating along the y-axis, the LET can be calculated with

$$\mathrm{LET} = \frac{W_{eh}\iiint N(x,y,z)\,dxdydz}{\rho t} \tag{2}$$
$$= \frac{W_{eh}2\pi}{\rho}\int_0^\infty N(r)r\,dr \tag{3}$$
$$= \frac{W_{eh}Q_0}{\rho t}, \tag{4}$$

where ρ the mass density, t thickness of the waveguide, and Q_0 is the carrier density integrated over the waveguide volume. The previously discussed assumption of uniform N in y direction and the radial definition were used to simplify the equation. While the LET is a measure derived from radiation studies on electronics, Q_0 is used in [21] in the analytical model of the OSET time evolution. Therefore, although this work focuses on the OSET at the time of the impact, the results could be useful for a time analysis as well. Examples of calculated LETs and Q_0 for the two previously shown ion species and four others are shown in Fig. 4(c). The simulation range goes from $0.1\,\mathrm{MeV/amu}$ to $100\,\mathrm{MeV/amu}$. This range was chosen because it captures the LET maxima of each species, which are commonly denoted as Bragg peaks. This peak can be seen in all the plotted curves in Fig. 4(c). On

This article has been accepted for publication in IEEE Transactions on Nuclear Science. This is the author's version which has not been fully edited and content may change prior to final publication. Citation information: DOI 10.1109/TNS.2024.3353489

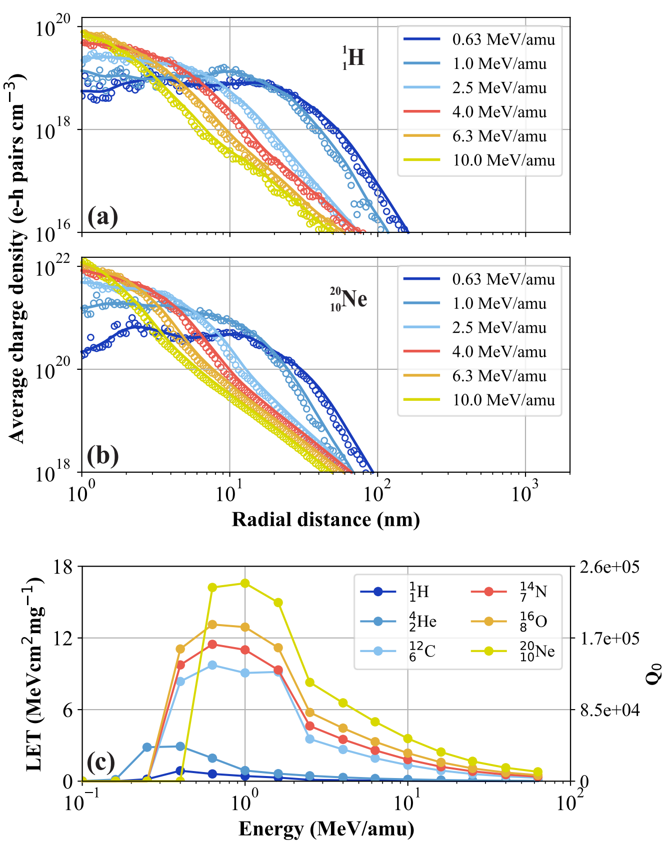

Fig. 4. EHP density generated by (a) $^1_1$H and (b) $^{20}_{10}$Ne for six different energies. The simulation (points) are filtered with a Gaussian moving average (line) to provide the FDTD simulation with a smoother carrier profile. (c) LET and Q_0 examples, calculated with (2).

its right side, the LET decreases slowly, while on its left side an abrupt drop to zero is usually found. At high energy, the charged particle has a small interaction cross section due to its high speed. As it slows down, corresponding to a lower initial energy, the interaction cross section increases. The peak of the interaction takes place when the particle has its lowest possible velocity in the Si layer, which here corresponds to a starting energy of about $1\,\mathrm{MeV/amu}$. Lower energies are not sufficient to penetrate the $2\,\mu\mathrm{m}$ thick SiO_2 cladding, and thus do not generate any charge in the waveguide. The LET and Q_0 are calculated for each simulation, i.e. for each (Z, E) pair.

C. FDTD Simulations

After the data set of ion tracks is generated, the next step is to calculate the resulting loss generated by each (Z, E) pair by performing 3D FDTD simulations in Meep [30], a free and open source software package for electromagnetic simulation. In this paper we consider $1550\,\mathrm{nm}$ as the operating wavelength for the communication payload. Historically the C-band, from $1530\,\mathrm{nm}$ to $1556\,\mathrm{nm}$, has been central to the development of optical fiber communication components, and is now also used for satellite optical communications [4]. Therefore, this is the wavelength range of choice for our analysis. The simulation is performed in the geometry shown in Fig. 1. After testing the simulation with different SiO_2 thicknesses, we considered sufficient to simulate only $140\,\mathrm{nm}$ on top and below the waveguide, and $275\,\mathrm{nm}$ on the sides. $3\,\mu\mathrm{m}$ is the chosen waveguide length, which is long enough to simulate the affected volume. Therefore, the final simulation volume dimensions are $2\,\mu\mathrm{m}\times1.5\,\mu\mathrm{m}\times4\,\mu\mathrm{m}$, that include the perfectly matched boundary conditions that are $0.5\,\mu\mathrm{m}$ thick. A mesh size of $4\,\mathrm{nm}$ was considered sufficient after testing lower mesh sizes. A Gaussian pulse centered at $\lambda = 1550\,\mathrm{nm}$ with a $20\,\mathrm{fs}$ full width at half maximum (FWHM) duration is injected into the simulation. The absorbed, transmitted, and reflected powers are simulated by computing the projection onto the waveguide's eigenmode. The phase shift is also extracted. First, the simulation is run without ion strike for reference. This reference simulation is needed to distinguish the intrinsic waveguide losses from the additional losses due to the ion strike. The strike location is $(x, y, z) = (0, 110, 0)$, meaning on the top of waveguide at its center. Lower losses are expected for a strike closer to the waveguide edge [22]. The filtered spatial distribution of the carriers $N(r)$ is converted into a change in the Si optical properties. As detailed in [20], at high carrier concentrations the Drude model without the weak-damping approximation needs to be used. Therefore, the general form of the Drude dielectric function ϵ is calculated and entered into the FDTD simulation. Furthermore, the refractive index n and the absorption losses α can be calculated using the relation $n + i\frac{\lambda}{4\pi}\alpha = \sqrt{\epsilon}$. With these new material properties, the simulation is re-run and the results are normalized to the reference simulation. An example of N, n, and α for $1\,\mathrm{MeV/amu}$ $^{80}_{35}$Br is shown in Fig. 5(a), Fig. 5(b), and Fig. 5(c), respectively. In this example, the largest change in n and α occurs in the first tens of nanometer from the impact location, and nominal properties are restored at a distance of about $200\,\mathrm{nm}$. The reflected, absorbed, and transmitted powers at $1550\,\mathrm{nm}$ are 0.07%, 5.14%, and 94.79%, respectively. These values are comparable with the transmissions measured in laser-induced OSET on Si waveguides [21], [24].

III. Results and Discussion

As discussed earlier, 35 different ion species were simulated in Geant4, and each one of them for different energies ranging from 0.1 to $100\,\mathrm{MeV/amu}$. Instead, only the energies in the range of 0.250 to $10\,\mathrm{MeV/amu}$ were simulated with FDTD simulations, since the absorption loss is smaller than 1% outside this range. For each (Z, E) pair, absorption (A), reflection (R) and transmission (T) were obtained from the 3D FDTD simulation. For the power budget analysis, the metric to look at is the excess signal loss, defined as: $L = 1 - T = R + A$. All the simulated losses are shown in Fig. 6(a), where they are plotted against the corresponding Z and E. L is low at low and high energies, maximum around $1\,\mathrm{MeV/amu}$, and it increases for larger atomic numbers. This was expected from the previous discussion: the ion energy is not sufficient to reach the buried Si waveguide at low energies, namely $E \lesssim 0.4\,\mathrm{MeV/amu}$, the maximum L occurs at the Bragg peak around $1\,\mathrm{MeV/amu}$, and L further decreases at higher energies due to the lower interaction cross section as seen in Fig. 4(c). For heavier ions,

This article has been accepted for publication in IEEE Transactions on Nuclear Science. This is the author's version which has not been fully edited and content may change prior to final publication. Citation information: DOI 10.1109/TNS.2024.3353489

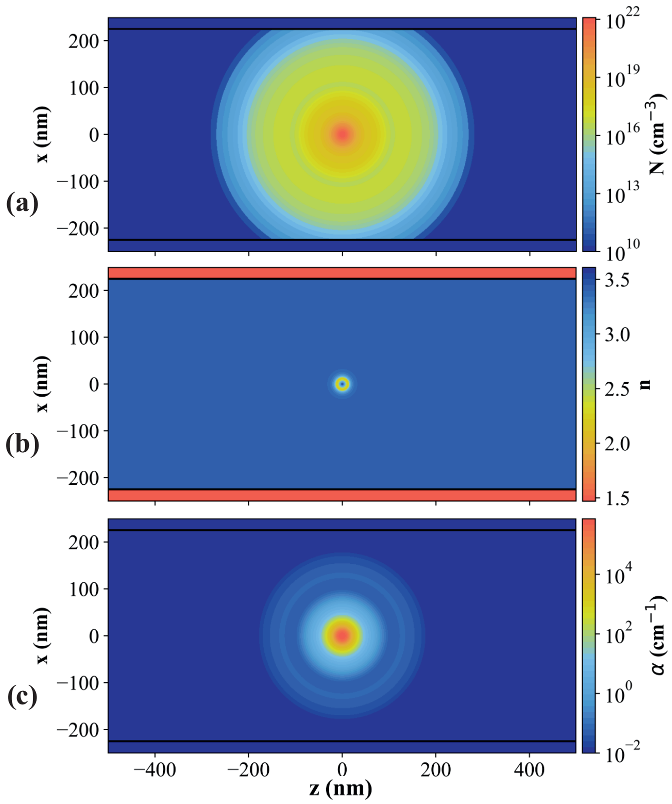

Fig. 5. (a) EHP density N after the impact of a $^{80}_{35}$Br with $1\,\mathrm{MeV/amu}$ energy, and corresponding (b) refractive index n and (c) absorption losses α. The 3D carrier distribution is obtained by rotating $N(r)$ around (x,z)=(0,0) and is truncated at the edges of the waveguide, as explained in [20].

the loss increases due to the increase in carrier concentration (seen in Fig. 4(a-b)), but it is limited to below 6.5% for the considered ions, corresponding to $0.29\,\mathrm{dB}$. For comparison, the expected channel loss in an optical feeder link varies between $73\,\mathrm{dB}$ to $89\,\mathrm{dB}$ [4]. Furthermore, no phase shift above $1.16°$ was extracted. Therefore, the OSET magnitudes for silicon waveguides require a small allocated link budget margin in the four studied satellite orbits and for a vertical ion strike.

The next step is to calculate the OSET rates. Here we are interested in calculating a cumulative rate $R(L_0)$, where R is the number of particles per second that generate a loss greater than L_0. In practice, given a L_0 that represents a perturbation threshold after which the link is disrupted, $R(L_0)$ is the disruption rate. First, given any L_0 and Z, the energy range $E^Z_{L_0^-} < E < E^Z_{L_0^+}$ in which $L > L_0$ is identified. Typically, $E^Z_{L_0^-}$ and $E^Z_{L_0^+}$ fall on the two sides of the Bragg peak. For every Z, i.e. for each row, an energy range can be identified, assuming that the ion can actually generate such loss. Then $R(L_0)$ is calculated using

$$R(L_0) = \sum_{Z=1}^{35} \int_{E^Z_{L_0^-}}^{E^Z_{L_0^+}} \frac{d\phi(Z,E)}{dE} \times A\, dE, \tag{5}$$

where the contributions of the different ion species are summed and the previously simulated differential flux $\frac{d\phi(Z,E)}{dE}$ is used. Thea area of $1\,\mathrm{cm}$ of waveguide is considered, which is $A = 1\,\mathrm{cm} \times 450\,\mathrm{nm} = 4.5 \times 10^{-5}\,\mathrm{cm}^2$. The cumulative OSET rates calculated for the four different orbits are plotted in Fig. 6(b-c). In Fig. 6(c), the fluxes that include the two solar flare models listed in Table II are shown. The worst-case solar flares are typically used to define an upper bound in a space radiation analysis. Starting from Fig. 6(b), we can observe that all OSET higher than 1% $(0.02\,\mathrm{dB})$ have a rate lower than $1 \times 10^{-6}\,\mathrm{s}^{-1}$, for all four orbits. This result strongly suggests that OSET will not be disruptive for the optical transmission in the waveguide. *GEO* and *Galileo* orbits suffer from higher radiation levels compared to LEO orbits, with *LEO-ISS* having the lowest rates. However, it is important to notice that in Section II-A we considered $1\,\mathrm{mm}$ Al shielding for all orbits in order to make a direct comparison. In practice, payloads on high altitude orbits such as *GEO* and *Galileo* have a thicker shielding and thus a lower rate than shown here. The worst case solar flare scenario in Fig. 6(c) shows an increase in rate of about three orders of magnitude. Nevertheless, the OSET rates are still lower than one per hour in almost all data points. A sudden drop at about 5.75% $(0.26\,\mathrm{dB})$ can be seen in both Fig. 6(b) and Fig. 6(c): this corresponds to the drop in RA at $Z > 26$ [15]. This confirms the robustness of Si photonic waveguides even during the worst-case scenario of a solar flare event.

Finally, it is interesting to discuss the relationship between the heavy ion LET and the induced loss. Previous studies have shown through simulation that $1 - T \sim e^{b \times LET}$ [20], where b was a fitting parameter. Fig. 7(a) shows the simulated ion strikes with energies between $0.63\,\mathrm{MeV/amu}$ - $6.3\,\mathrm{MeV/amu}$, where $L = 1 - T$ is plotted against the calculated LET and Q_0. The data points are grouped for the different energies per amu, because we expect the carrier distributions to be similar within each set, as previously shown in Fig. 4(a-b) and discussed in [27]. It is clear from Fig. 7(a) that there is no one-to-one relationship between $1 - T$ and LET, contrary to what was shown in [20]. Instead, for any LET, i.e. for the same amount of generated charge Q_0, the resulting loss depends on the ion energy. The result in [20] was concluded from a limited set of ion tracks, while in this work a larger set of simulations was used. From Fig. 7(a), we can also see that the energies close the Bragg peak $(0.63\,\mathrm{MeV/amu}$, $1\,\mathrm{MeV/amu}$, and $1.6\,\mathrm{MeV/amu})$ give the fastest increase in loss. Beyond this point, the higher the energy, the slower the increase. To further investigate this behavior, the carrier distributions with $\mathrm{LET} \approx 30\,\mathrm{MeVcm^2mg^{-1}}$ are compared in Fig. 7(b), where the optical mode in the waveguide is shown with a red line. These distributions are taken at $z = 0$, meaning the waveguide cross-section at the impact location is considered. The high energy ions have a distribution that is concentrated in a small fraction of the optical power and that has a rapid decay with radial distance from the impact site. Instead, the lower energies have a slower decay. Therefore, we can conclude that not only the total amount of generated carriers plays an important role, but also their distribution needs to be taken into account in the initial loss.

These results can be compared to SEE studies on electronics. Over the past two decades, several studies have

This article has been accepted for publication in IEEE Transactions on Nuclear Science. This is the author's version which has not been fully edited and content may change prior to final publication. Citation information: DOI 10.1109/TNS.2024.3353489

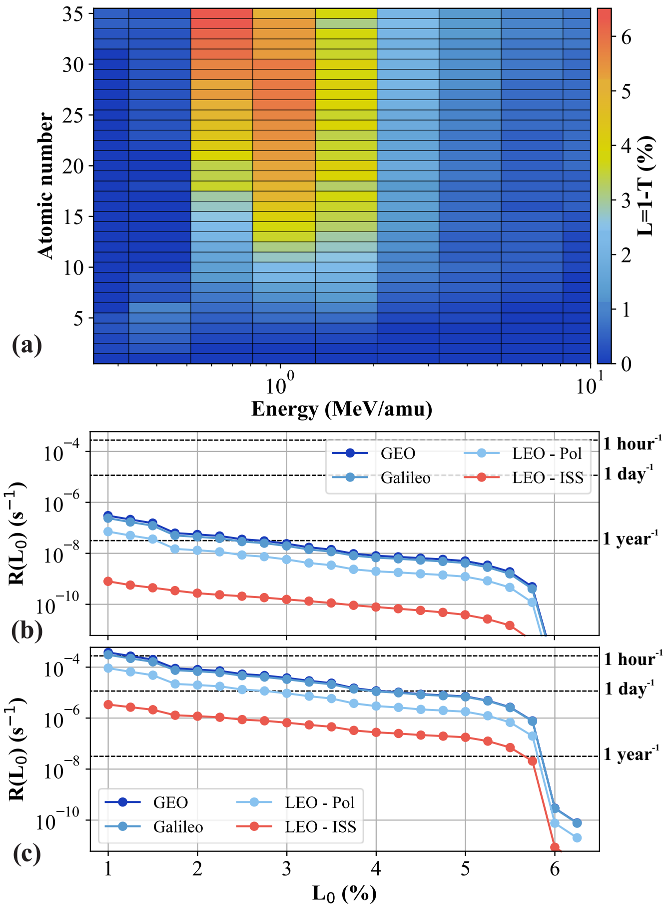

Fig. 6. (a) Simulated excess loss L versus heavy ion atomic number and energy. Cumulative OSET rates for different loss thresholds L_0, (b) without and (c) with solar flare. Thresholds of one per hour/day/year are indicated.

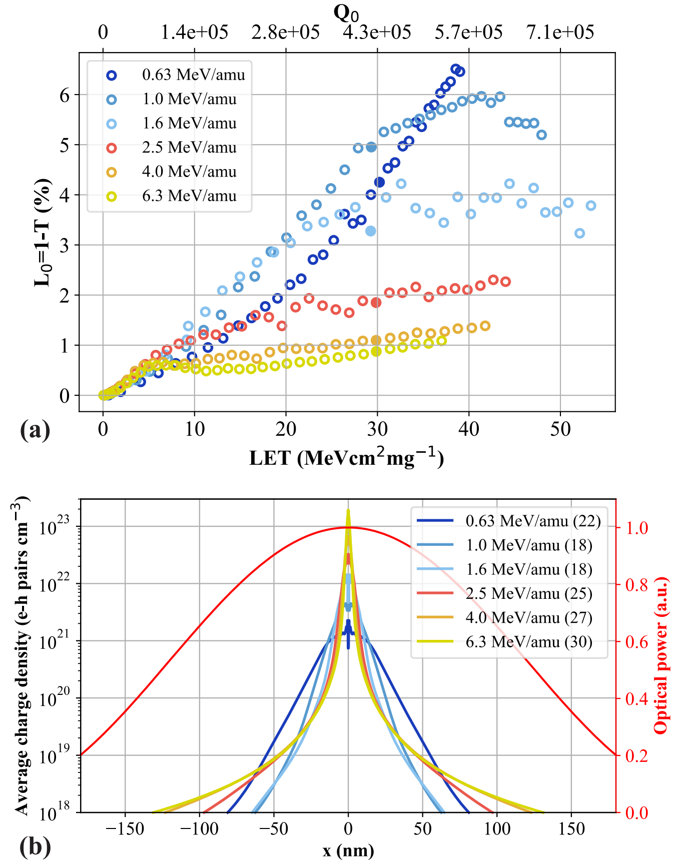

Fig. 7. (a) $1 - T$ versus calculated LET and Q_0 of the simulated ions in the energy range of $0.63\,\mathrm{MeV/amu}$ to $6.3\,\mathrm{MeV/amu}$. (b) Average charge density distribution in the waveguide cross section for the ions with filled circle in (a) (left y-axis), compared to the optical power of the fundamental mode (red line, right y-axis). Each line is labeled with the ion energy and its atomic number in paranthesis.

highlighted that LET on its own is not always an accurate metric for predicting SEE [38]–[40]. With the miniaturization and integration of electronics, the radial distribution of the generated charges started to play an important role, as the dimensions became comparable. We could make a similar conclusion for integrated photonics: the optical mode wavelength in the considered Si photonic waveguide is $\lambda = \lambda_0/n_{\mathrm{Si}} = 1550/3.48 \approx 445\,\mathrm{nm}$, thus comparable to the length scales of the ion track, typically few hundreds of nm. Therefore, we could expect the radial distribution to play an important role in integrated photonics as well, as shown in Fig. 7(a). Nevertheless, this analysis is still limited by the simplifications of an ion with a perpendicular trajectory striking in the center of the waveguide, and by the simplification of only looking at the initial OSET. To have a more conclusive picture about the relationship between the LET and the OSET, one would need to look at OSETs with same LET and different angles, and at the time evolution of OSETs with the same LET. For instance, the same Q_0 might result in the same loss once the initial EHP distribution is smoothed out by ambipolar diffusion.

IV. Conclusions

In this work, a framework to simulate OSET rates and magnitudes on Si photonic waveguides for specific satellite orbits was presented. Three open-source tools (OMERE [28], Geant4 [29] and Meep [30]) were used, thus making this approach widely available compared to the use of commercial tools. With this combination, it was possible to investigate the effects of heavy ions for a realistic radiation environment. This can benefit the C-SWaP of optical communication payloads, as the calculated OSETs can be used for a more accurate link budget calculation. Furthermore, the modular approach of the simulations makes it easy to evaluate the effect on other satellite orbits, or to investigate other photonic devices, since only the relevant simulation step needs to be re-run (see Fig. 2).

To present the framework, we first simulated four typical satellite orbits in OMERE, and obtained differential fluxes for a wide range of atomic numbers and energies. Only the elements with atomic number $Z < 35$ were considered for the following steps, due to the interactions with heavier ions being so rare that their impact on the results is negligible. Then, realistic carrier distributions were generated with a Geant4 simulation. The distributions were then converted into changes of material properties using the Drude model [20], and 3D FDTD simulations were used to compute the power loss through the waveguide. Finally, OSET rates and

This article has been accepted for publication in IEEE Transactions on Nuclear Science. This is the author's version which has not been fully edited and content may change prior to final publication. Citation information: DOI 10.1109/TNS.2024.3353489

magnitudes were calculated. The results showed that power losses above 6.5% are highly unlikely for the considered satellite orbits and a vertical ion strike. Therefore, OSETs in Si photonic waveguides do not appear to be a concern for silicon photonics-based OSL communication. Furthermore, the role of LET for OSET was investigated. We showed that the same LET, corresponding to the same Q_0, can lead to very different losses, thus indicating that this metric alone might not be accurate enough for studying radiation effects on a photonic device. The importance of considering the overlap of the carrier distribution with the optical mode was also discussed.

The next steps are to investigate angled trajectories, to understand the effects of a trajectory that has a longer path through the waveguide, and to include the time evolution of the losses. For instance, it would important to understand how the losses are evolving in time when the carriers are both absorbed and diffused. After that, other important photonic devices could be simulated, such as multimode interferometers (MMIs), and directional couplers. Intuitively, we expect that in devices where the optical mode is broadened, such as MMIs, the effect of heavy ion will be reduced due to less overlap with the carrier distributions. Other steps include testing more computationally efficient approaches. For example, perturbation theory could be used instead of FDTD simulations [22], or the Z^2 scaling of the carrier distribution could be used to reduce the number of Geant4 simulations required [27]. Finally. the framework could be integrated with OSET time domain descriptions [21], [22] starting from the calculated Q_0.

Acknowledgment

We thank Samuele Raffa for useful discussions on the radiation topic. We acknowledge the use of the following open source tools: OMERE [28], Geant4 [29], [35] and Meep [30].

References

[1] H. Kaushal and G. Kaddoum, "Optical Communication in Space: Challenges and Mitigation Techniques," *IEEE Communications Surveys Tutorials*, vol. 19, no. 1, pp. 57–96, Feb. 2017.

[2] H. Hauschildt, S. Mezzasoma, H. L. Moeller, M. Witting, and J. Herrmann, "European data relay system goes global," in *2017 IEEE International Conference on Space Optical Systems and Applications (ICSOS)*, pp. 15–18, 2017.

[3] A. Biswas, M. Srinivasan, R. Rogalin, S. Piazzolla, J. Liu, B. Schratz, A. Wong, E. Alerstam, M. Wright, W. T. Roberts, J. Kovalik, G. Ortiz, A. Na-Nakornpanom, M. Shaw, C. Okino, K. Andrews, M. Peng, D. Orozco, and W. Klipstein, "Status of NASA's deep space optical communication technology demonstration," in *2017 IEEE International Conference on Space Optical Systems and Applications (ICSOS)*, pp. 23–27, 2017.

[4] R. M. Calvo, J. Poliak, J. Surof, A. Reeves, M. Richerzhagen, H. F. Kelemu, R. Barrios, C. Carrizo, R. Wolf, F. Rein, A. Dochhan, K. Saucke, and W. Luetke, "Optical technologies for very high throughput satellite communications," in *Free-Space Laser Communications XXXI* (H. Hemmati and D. M. Boroson, eds.), vol. 10910, pp. 189 – 204, International Society for Optics and Photonics, SPIE, 2019.

[5] Benjamin Rödiger and Christian Menninger and Christian Fuchs and Lukas Grillmayer and Saskia Arnold and Christoph Rochow and Philipp Wertz and Christopher Schmidt, "High data-rate optical communication payload for CubeSats," in *Laser Communication and Propagation through the Atmosphere and Oceans IX* (J. A. Anguita, J. P. Bos, and D. T. Wayne, eds.), vol. 11506, pp. 12 – 24, International Society for Optics and Photonics, SPIE, 2020.

[6] P. Conroy, J. Surof, J. Poliak, and R. M. Calvo, "Demonstration of 40 GBaud intradyne transmission through worst-case atmospheric turbulence conditions for geostationary satellite uplink," *Appl. Opt.*, vol. 57, no. 18, pp. 5095–5101, June 2018.

[7] J. Poliak, R. M. Calvo, and F. Rein, "Demonstration of 1.72 Tbit/s Optical Data Transmission Under Worst-Case Turbulence Conditions for Ground-to-Geostationary Satellite Communications," *IEEE Communications Letters*, vol. 22, no. 9, pp. 1818–1821, Sep. 2018.

[8] H. Zhao, S. Pinna, B. Song, L. Megalini, S. T. š. Brunelli, L. A. Coldren, and J. Klamkin, "Indium Phosphide Photonic Integrated Circuits for Free Space Optical Links," *IEEE Journal of Selected Topics in Quantum Electronics*, vol. 24, no. 6, pp. 1–6, Nov. 2018.

[9] M. Ziarko, G. Terrasanta, and R. M. Calvo, "Optical Communications for Very High Throughput Satellites," in *OSA Advanced Photonics Congress 2021*, p. NeTh2C, Optica Publishing Group, 2021.

[10] P. Marin-Palomo, J. N. Kemal, M. Karpov, A. Kordts, J. Pfeifle, M. H. Pfeiffer, P. Trocha, S. Wolf, V. Brasch, M. H. Anderson, R. Rosenberger, K. Vijayan, W. Freude, T. J. Kippenberg, and C. Koos, "Microresonator-based solitons for massively parallel coherent optical communications," *Nature*, vol. 546, no. 7657, pp. 274–279, June 2017.

[11] A. A. Jørgensen, D. Kong, M. R. Henriksen, F. Klejs, Z. Ye, Ã. B. Helgason, H. E. Hansen, H. Hu, M. Yankov, S. Forchhammer, P. Andrekson, A. Larsson, M. Karlsson, J. Schröder, Y. Sasaki, K. Aikawa, J. W. Thomsen, T. Morioka, M. Galili, V. Torres-Company, and L. K. Oxenløwe, "Petabit-per-second data transmission using a chip-scale microcomb ring resonator source," *Nature Photonics*, vol. 16, no. 11, pp. 798–802, Nov. 2022.

[12] F. Kish, V. Lal, P. Evans, S. W. Corzine, M. Ziari, T. Butrie, M. Reffle, H. Tsai, A. Dentai, J. Pleumeekers, M. Missey, M. Fisher, S. Murthy, R. Salvatore, P. Samra, S. Demars, N. Kim, A. James, A. Hosseini, P. Studenkov, M. Lauermann, R. Going, M. Lu, J. Zhang, J. Tang, J. Bostak, T. Vallaitis, M. Kuntz, D. Pavinski, A. Karanicolas, B. Behnia, D. Engel, O. Khayam, N. Modi, M. R. Chitgarha, P. Mertz, W. Ko, R. Maher, J. Osenbach, J. T. Rahn, H. Sun, K. Wu, M. Mitchell, and D. Welch, "System-on-Chip Photonic Integrated Circuits," *IEEE Journal of Selected Topics in Quantum Electronics*, vol. 24, no. 1, pp. 1–20, Jan. 2018.

[13] D. Thomson, A. Zilkie, J. E. Bowers, T. Komljenovic, G. T. Reed, L. Vivien, D. Marris-Morini, E. Cassan, L. Virot, J.-M. Fédéli, J.-M. Hartmann, J. H. Schmid, D.-X. Xu, F. Boeuf, P. O'Brien, G. Z. Mashanovich, and M. Nedeljkovic, "Roadmap on silicon photonics," *Journal of Optics*, vol. 18, no. 7, p. 073003, June 2016.

[14] G. N. Tzintzarov, S. G. Rao, and J. D. Cressler, "Integrated Silicon Photonics for Enabling Next-Generation Space Systems," *Photonics*, vol. 8, no. 4, April 2021.

[15] S. Bourdarie and M. Xapsos, "The Near-Earth Space Radiation Environment," *IEEE Transactions on Nuclear Science*, vol. 55, no. 4, pp. 1810–1832, April 2008.

[16] F. Sexton, "Destructive single-event effects in semiconductor devices and ICs," *IEEE Transactions on Nuclear Science*, vol. 50, no. 3, pp. 603–621, June 2003.

[17] D. Munteanu and J.-L. Autran, "Modeling and Simulation of Single-Event Effects in Digital Devices and ICs," *IEEE Transactions on Nuclear Science*, vol. 55, no. 4, pp. 1854–1878, Aug. 2008.

[18] D. Kobayashi, "Scaling Trends of Digital Single-Event Effects: A Survey of SEU and SET Parameters and Comparison With Transistor Performance," *IEEE Transactions on Nuclear Science*, vol. 68, no. 2, pp. 124–148, Feb. 2021.

[19] Y. Liu and H. K. Tsang, "Time dependent density of free carriers generated by two photon absorption in silicon waveguides," *Applied Physics Letters*, vol. 90, no. 21, p. 211105, May 2007.

[20] P. S. Goley, Z. E. Fleetwood, and J. D. Cressler, "Potential Limitations on Integrated Silicon Photonic Waveguides Operating in a Heavy Ion Environment," *IEEE Transactions on Nuclear Science*, vol. 65, no. 1, pp. 141–148, Jan. 2018.

[21] P. S. Goley, G. M. Maggioni, E. Preisler, and J. D. Cressler, "Modeling transient loss due to ionizing particles in silicon photonic waveguides," *IEEE Transactions on Nuclear Science*, vol. 69, no. 3, pp. 518–526, March 2022.

[22] L. D. Ryder, R. D. Schrimpf, R. A. Reed, and S. M. Weiss, "Radiation-Induced Transient Response Mechanisms in Photonic Waveguides," *IEEE Transactions on Nuclear Science*, vol. 69, no. 3, pp. 546–557, Feb. 2022.

[23] R. C. Boggs, E. Richards, L. W. Massengill, and T. D. Loveless, "An Electro-Optical Simulation Methodology for the Analysis of Single-Event Radiation Effects in Photonic Devices," in *2019 SoutheastCon*, pp. 1–5, April 2019.

[24] G. N. Tzintzarov, A. Ildefonso, J. W. Teng, M. Frounchi, A. Djikeng, P. Iyengar, P. S. Goley, A. Khachatrian, J. Hales, R. Bahr, S. P. Buchner, D. Mcmorrow, and J. D. Cressler, "Optical Single-Event Transients Induced in Integrated Silicon-Photonic Waveguides by Two-Photon Absorption," *IEEE Transactions on Nuclear Science*, vol. 68, no. 5, pp. 785–792, Jan. 2021.

[25] L. D. Ryder, K. L. Ryder, A. L. Sternberg, J. A. Kozub, E. X. Zhang, D. Linten, K. Croes, R. A. Weller, R. D. Schrimpf, S. M. Weiss, and R. A. Reed, "Single-Event Transient Response of Vertical and Lateral Waveguide-Integrated Germanium Photodiodes," *IEEE Transactions on Nuclear Science*, vol. 68, no. 5, pp. 801–806, Jan. 2021.

[26] G. N. Tzintzarov, J. W. Teng, A. N. Bozovich, G. R. Allen, D. Nergui, Y. A. Mensah, and J. D. Cressler, "Single-Event Transients in a Commercially Available, Integrated Germanium Photodiode for Silicon Photonic Systems," *IEEE Transactions on Nuclear Science*, vol. 69, no. 3, pp. 527–533, March 2022.

[27] M. Raine, M. Gaillardin, P. Paillet, and O. Duhamel, "Towards a Generic Representation of Heavy Ion Tracks to be Used in Engineering SEE Simulation Tools," *IEEE Transactions on Nuclear Science*, vol. 61, no. 4, pp. 1791–1798, August 2014.

[28] P. Peyrard, T. Beutier, O. Serres, C. Chatry, R. Ecoffet, G. Rolland, D. Boscher, S. Bourdarie, C. Inguimbert, P. Calvel, *et al.*, "OMERE 2.0 a toolkit for space environment," in *IEEE Proceedings of the 7th European Conference on Radiation and its Effects on Components and Systems RADECS*, pp. 639–641, 2003.

[29] J. Allison, K. Amako, J. Apostolakis, H. Araujo, P. Arce Dubois, M. Asai, G. Barrand, R. Capra, S. Chauvie, R. Chytracek, G. Cirrone, G. Cooperman, G. Cosmo, G. Cuttone, G. Daquino, M. Donszelmann, M. Dressel, G. Folger, F. Foppiano, J. Generowicz, V. Grichine, S. Guatelli, P. Gumplinger, A. Heikkinen, I. Hrivnacova, A. Howard, S. Incerti, V. Ivanchenko, T. Johnson, F. Jones, T. Koi, R. Kokoulin, M. Kossov, H. Kurashige, V. Lara, S. Larsson, F. Lei, O. Link, F. Longo, M. Maire, A. Mantero, B. Mascialino, I. McLaren, P. Mendez Lorenzo, K. Minamimoto, K. Murakami, P. Nieminen, L. Pandola, S. Parlati, L. Peralta, J. Perl, A. Pfeiffer, M. Pia, A. Ribon, P. Rodrigues, G. Russo, S. Sadilov, G. Santin, T. Sasaki, D. Smith, N. Starkov, S. Tanaka, E. Tcherniaev, B. Tome, A. Trindade, P. Truscott, L. Urban, M. Verderi, A. Walkden, J. Wellisch, D. Williams, D. Wright, and H. Yoshida, "Geant4 developments and applications," *IEEE Transactions on Nuclear Science*, vol. 53, no. 1, pp. 270–278, Feb. 2006.

[30] A. F. Oskooi, D. Roundy, M. Ibanescu, P. Bermel, J. Joannopoulos, and S. G. Johnson, "Meep: A flexible free-software package for electromagnetic simulations by the FDTD method," *Computer Physics Communications*, vol. 181, no. 3, pp. 687–702, March 2010.

[31] N. Pachler, I. del Portillo, E. F. Crawley, and B. G. Cameron, "An Updated Comparison of Four Low Earth Orbit Satellite Constellation Systems to Provide Global Broadband," in *2021 IEEE International Conference on Communications Workshops (ICC Workshops)*, pp. 1–7, 2021.

[32] ECSS, "Space envirnoment," *ECSS-E-ST-10-04C Rev. I*, 2019.

[33] ECSS, "Space envirnoment," *ECSS-E-ST-10-04C Rev. I*, 2020.

[34] G. Kraft, M. Krämer, and M. Scholz, "LET, track structure and models," *Radiation and environmental biophysics*, vol. 31, no. 3, pp. 161–180, Sep. 1992.

[35] A. Valentin, M. Raine, M. Gaillardin, and P. Paillet, "Geant4 physics processes for microdosimetry simulation: Very low energy electromagnetic models for protons and heavy ions in silicon," *Nuclear Instruments and Methods in Physics Research Section B: Beam Interactions with Materials and Atoms*, vol. 287, pp. 124–129, Sep. 2012.

[36] M. Raine, A. Valentin, M. Gaillardin, and P. Paillet, "Improved Simulation of Ion Track Structures Using New Geant4 Models—Impact on the Modeling of Advanced Technologies Response," *IEEE Transactions on Nuclear Science*, vol. 59, no. 6, pp. 2697–2703, Dec. 2012.

[37] Q. Gibaru, C. Inguimbert, P. Caron, M. Raine, D. Lambert, and J. Puech, "Geant4 physics processes for microdosimetry and secondary electron emission simulation: Extension of MicroElec to very low energies and 11 materials (C, Al, Si, Ti, Ni, Cu, Ge, Ag, W, Kapton and SiO2)," *Nuclear Instruments and Methods in Physics Research Section B: Beam Interactions with Materials and Atoms*, vol. 487, pp. 66–77, Jan. 2021.

[38] R. A. Reed, R. A. Weller, M. H. Mendenhall, J.-M. Lauenstein, K. M. Warren, J. A. Pellish, R. D. Schrimpf, B. D. Sierawski, L. W. Massengill, P. E. Dodd, M. R. Shaneyfelt, J. A. Felix, J. R. Schwank, N. F. Haddad, R. K. Lawrence, J. H. Bowman, and R. Conde, "Impact of Ion Energy and Species on Single Event Effects Analysis," *IEEE Transactions on Nuclear Science*, vol. 54, no. 6, pp. 2312–2321, Dec. 2007.

[39] M. P. King, R. A. Reed, R. A. Weller, M. H. Mendenhall, R. D. Schrimpf, M. L. Alles, E. C. Auden, S. E. Armstrong, and M. Asai, "The Impact of Delta-Rays on Single-Event Upsets in Highly Scaled SOI SRAMs," *IEEE Transactions on Nuclear Science*, vol. 57, no. 6, pp. 3169–3175, Dec. 2010.

[40] M. Raine, G. Hubert, M. Gaillardin, L. Artola, P. Paillet, S. Girard, J.-E. Sauvestre, and A. Bournel, "Impact of the Radial Ionization Profile on SEE Prediction for SOI Transistors and SRAMs Beyond the 32-nm Technological Node," *IEEE Transactions on Nuclear Science*, vol. 58, no. 3, pp. 840–847, June 2011.